Impacts of aerosol-monsoon interaction on rainfall and circulation over Northern India and the Himalaya Foothills

William K. M. Lau[1,2], Kyu-Myong Kim[3], Jainn-Jong Shi[4], T. Matsui[1], M. Chin[5], Qian Tan[5], C. Peters-Lidard[6], and W. K. Tao[7]

[1]*Earth System Science Interdisciplinary Center (ESSIC),*
U. of Maryland, College Park, Md 20740
[2]*Department of Atmospheric Sciences, U. of Texas, Station College, TX, 77843.*
[3]*Climate and Radiation Laboratory, Earth Science Division,*
Goddard Space Flight Center, Greenbelt, MD, 20771
[4] *Goddard Earth Science Technology, Application Research (GESTAR),*
Morgan State University, Baltimore, MD, 21251
[5]*Atmospheric Chemistry and Dynamics Laboratory, Earth Science Division,*
Goddard Space Flight Center, Greenbelt, MD, 20771
[6]*Earth Science Division, Goddard Space Flight Center, Greenbelt, MD, 20771*
[7]*Mesoscale Atmospheric Processes Laboratory, Earth Science Division,*
Goddard Space Flight Center, Greenbelt, MD., 20771

29 **Abstract**
30
31   The boreal summer of 2008 was unusual for the Indian monsoon, featuring exceptional

32 heavy loading of dust aerosols over the Arabian Sea and northern-central India, near normal all-

33 India rainfall, but excessive heavy rain, causing disastrous flooding in the Northern Indian

34 Himalaya Foothills (NIHF) regions, accompanied by persistent drought conditions in central and

35 southern India.   Using NASA Unified-physics Weather Research Forecast (NUWRF) model

36 with fully interactive aerosol physics and dynamics, we carried out three sets of 7-day ensemble

37 model forecast experiments: 1) control with no aerosol, 2) aerosol radiative effect only and 3)

38 aerosol radiative and aerosol-cloud-microphysics effects, to study the impacts of aerosol-

39 monsoon interactions on monsoon variability over the NIHF during the summer of 2008.

40 Results show that aerosol-radiation interaction (ARI), *i.e.*, dust aerosol transport, and dynamical

41 feedback processes induced by aerosol-radiative heating, plays a key role in altering the large-

42 scale monsoon circulation system, reflected by an increased north-south tropospheric

43 temperature gradient, a northward shift of heavy monsoon rainfall, advancing the monsoon onset

44 by 1-5 days over the HF, consistent with the EHP hypothesis (Lau et al. 2006).   Additionally, we

45 found that dust aerosols, via the semi-direct effect, increase atmospheric stability, and cause the

46 dissipation of a developing monsoon onset cyclone over northeastern India/northern Bay of

47 Bengal. Eventually, in a matter of several days, ARI transforms the developing monsoon

48 cyclone into meso-scale convective cells along the HF slopes. Aerosol-Cloud-microphysics

49 Interaction (ACI) further enhances the ARI effect in invigorating the deep convection cells and

50 speeding up the transformation processes.   Results indicate that even in short-term (up to

51 weekly) numerical forecasting of monsoon circulation and rainfall, effects of aerosol-monsoon

52 interaction can be substantial and cannot be ignored.

53

1. Introduction

The Northern India and Himalayan foothills (NIHF) region is an essential component of the Indian monsoon (Gadgil et al. 2003). Summer monsoon rainfall over this region feeds the Ganges, and the Indus rivers, providing fresh water essential for agriculture, industrial and livelihood over hundreds of millions people in the region. The Himalayan foothills (HF), an escarpment that rises to over 5 km above the Indo-Gangetic Plain (IGP) over Northern India (NI), provides a major barrier to the northward advance of the Indian monsoon rainfall, as well as contributing to the thermal contrast between the Tibetan Plateau and the Indian Ocean (Boos and Kuang 2010; Wu et al. 2012). It also provides strong orographic forcing to the prevailing southwesterly monsoon flow, giving rise to strong vertical ascent and development of vigorous thunderstorm cells with intense precipitation during the monsoon season (Houze *et al*. 2007; Rasmusson and Houze 2012; Das *et al*. 2014). The importance of the NIHF orography in forcing strong convection and extreme precipitations, in relationship to the large-scale Indian monsoon has also been reported (Barros and Lang 2003; Barros and Lattenmaier 1994).

Recently, an increasing number of studies have suggested that absorbing aerosols (mainly desert dusts and carbonaceous aerosols) can affect the interannual and intraseasonal variability of the Indian monsoon rainfall (Lau et al. 2006; Lau and Kim 2006; Manoj et al. 2011; Hazra et al. 2013; Vinoj et al. 2014; Kim et al. 2015; D'Errico et al. 2015; Sanap and Pandithurai 2015, and many others). Based on these studies, Lau (2016) has proposed a new paradigm arguing that natural aerosol, particularly dust and carbonaceous aerosols from natural sources should be considered an essential component of an intrinsic aerosol-monsoon weather and climate system. Specifically for the NIHF region, the Elevated Heat Pump

77 (EHP) hypothesis (Lau et al. 2006) posited that through atmospheric diabatic heating and

78 circulation feedbacks, atmospheric heating due to absorbing aerosols from both

79 anthropogenic and natural sources accumulated over the Indo-Gangetic Plain during the pre-

80 monsoon period can, lead to increased rainfall and advance of the monsoon rainy season over

81 the NIHF. At present, effects of absorbing aerosols in increasing monsoon rainfall and

82 circulation consistent with EHP, but with significantly different regional spatial and temporal

83 details have been found in many global climate models (Lau et al. 2006; Meehl et al. 2008;

84 Randles and Ramawamy 2008; Wang et al. 2009; Collier and Zhang 2009; Henriksson, et al.

85 2014; D' Errico et al. 2015, Jin et al. 2015). One of the main reasons for the regional

86 differences is that state-of-the-art climate models, due to their coarse resolution generally, are

87 still unable to resolve the complex topography and interactions of monsoon winds,

88 precipitation and aerosol transport, sources and sink processes over the NIHF.   For more

89 realistic simulations, the use of high-resolution regional atmospheric model with realistic

90 representation of aerosol and monsoon processes is required. In this paper, using the NASA

91 Unified Physics Weather Research Forecast (NU-WRF) model, we have carried out

92 numerical experiments aimed at providing a better understanding of the physical processes

93 involved in aerosol-monsoon interactions, including aerosol radiative and microphysical

94 effects, as well as induced dynamical feedbacks over the complex topography of the NIHF

95 region.   The experiments will be conducted based on a case study of the 2008 Indian

96 monsoon.

97

98 *1.1   The 2008 Indian monsoon*

99   The all-Indian monsoon rainfall for the full monsoon season (June-September) during

100   2008 was near normal. However, rainfall was excessive in the north, but deficient in the

101   central and southern India for most of the season (Rao et al. 2011). Abnormally heavy rain

102   started in early June, and lasted through early August. The heavy rainfall eventually led to

103   the breaching of the Kosi river in early August, with disastrous flooding over Nepal and

104   many states in northern India including, Assam, Andhra Pradesh, Bihar, Maharashtra, Uttar

105   Pradesh, West Bengal and Orissa.   The flood affected over 2.3 million people in the northern

106   part of the state of Bihar, prompting the Indian government to declare a national

107   disaster.   The heavy rain in June (Fig. 1a) was found mainly over NIHF, extending

108   southeastward toward the Bay of Bengal.   At the same time, rainfall was suppressed over

109   southwestern, central and southern, and extreme northeastern India. The summer of 2008

110   also witnessed an early onset of the monsoon over northern India (Tyagi et al. 2009). Most

111   interesting, it was also a year with unusually large loading of aerosols over the Arabian Sea,

112   northwestern India, and across central Indian during the early monsoon season (Fig. 1b).   In

113   this study, we will examine the possible roles of aerosols in influencing this rather unusual

114   Indian monsoon.

115

116   **2. Modeling strategy and methodology**

117   We use the NASA Unified physics Weather Research Forecast (NUWRF)

118   regional atmospheric model to carry out ensemble forecast experiments to investigate the

119   role of aerosol-monsoon dynamic interaction in the NIHF region. NUWRF has been

120   developed at GSFC to unify physics in WRF with NASA's current physics package for

121   aerosol and cloud microphysics, as well as assimilation systems, common to GEOS-5, the

122   Goddard Cumulus Ensemble cloud model (GCE) (Tao et al. 2009), the Goddard

123   Chemistry and Radiation Transport (GOCART) model (Chin et al. 2004, 2009, 2014,

124   Ginoux et al. 2001), and the Land data Information System (LIS) (Peters-Lidard et al.

125   2007, 2015, Tao et al. 2013, Lang et al. 2014, Shi et al. 2014). Briefly, GOCART uses

126   the following modules in aerosol simulation: emission, which includes dust, sulfur, black

127   carbon, organic carbon, and sea-salt emissions; chemistry, which includes in-air and in-

128   cloud oxidations of sulfate precursors (SO_2 and DMS); turbulent dry deposition, which is

129   calculated by aerodynamic resistance; gravitational settling, which is a function of air

130   viscosity and particle size; and wet deposition, which accounts for the scavenging of

131   soluble species in convective updrafts and rainout/washout in large-scale precipitation.

132   Dust size distribution is calculated by solving the continuity equation for eight size bins

133   ranging from 0.1 to 10 μm in radii, representing mineral dust types from fine clay to

134   coarse sand particles. The continuity equation includes macroscopic advection by winds,

135   parameterized eddy diffusion and moist convection. The removal mechanisms include

136   dry deposition at the surface by impaction, wet deposition in and below clouds, and

137   gravitational settling. Dust emission is computed as a function of the surface wind at 10

138   m, a threshold frictional velocity, and a source function which is depended on

139   geographic locations and dust sizes (Ginaux et al. 2001, Gillette and Passi 1988).

140   For aerosol-cloud microphysics, NUWRF computes cloud droplet concentration

141   using aerosol mass directly predicted by GOCART/WRF-Chem at each time step. For a

142   given air temperature and supersaturation, cloud condensation nuclei (CCN) is calculated

143   from the aerosol species predicted by GOCART based on the Koehler curve (Koehler et al.

144   2006, Andreae and Rosenfeld 2008), while the concentration of ice nuclei (IN) is obtained

145   following the approach of DeMott et al. (2010). Both CCN and IN are diagnostic parameters

146   calculated from the WRF-Chem/GOCART-predicted aerosol mass concentrations in the

147   Goddard one-moment microphysics scheme. CCN is used to calculate the auto-conversion

148   of cloud liquid water (Qc) to rain water (Qr) following Liu and Daum (2004), while IN is

149   used to calculate 1) the conversion of cloud ice (Qi) to snow (Qs) due to the Bergeron

150   process and 2) the growth of cloud liquid water (Qc) to cloud ice (Qi) due to deposition.

151   The NUWRF team has also coupled GOCART with LIS which provides key

152   information (e.g., soil moisture and soil porosity) that GOCART uses to calculate dust

153   emissions. GOCART has also been coupled with the Goddard radiation and microphysics

154   scheme to simulate the direct and indirect aerosol effects on energy budget, cloud, and

155   precipitation. Parameterization schemes to estimate biogenic secondary organic aerosols have

156   also been integrated from WRF/Chem into NUWRF.   In addition, several model utilities

157   have been developed and modified to facilitate NUWRF applications, including

158   implementation of time varying GOCART aerosols types and distribution as initial and

159   boundary conditions, and incorporation of pollutant emissions inventories for both

160   anthropogenic and natural sources. For the present experiments, the single scattering albedo

161   of dust aerosol at the visible band (0.4-0.7 μm) were specified in the range 0.95 to 0.79,

162   representing 8 size categories of dust from fine clay to coarse dust particles. The much

163   higher absorption (lower single scattering albedo) for larger size particles is consistent with

164   recent observations indicating coating of fine black carbon particle on the larger size sand

165   particles in Asian monsoon regions (Ganguly et al., 2005, Satheesh and Ramanathan 2008,

166   Eck et al., 2010)

167   For our model experiments, we followed the ensemble forecast methodology

168   commonly used for monsoon numerical weather prediction up to a week to investigate the

169   impacts of aerosol-monsoon dynamic interaction on short time scales. We used nested

170   domains with 9 km resolution in an inner domain (60-100°E, 10-40°N) covering the Indian

171   subcontinent and eastern Indo-China, and an outer domain with 27 km resolution, spanning

172   the large-scale monsoon domain (40-120° E, 5°S-40°N), with 61 layers in the vertical (Fig.

173   S1). We selected the early monsoon period June 1- July 15 2008 for our study.   This period

174   covered the monsoon onset transition phase (June 11-17), and several subsequent heavy rain

175   events over NIHF (See discussion in Section 2.1). We carried out 45, 7-day forecast

176   experiments forced by prescribed observed sea surface temperature, at intervals of one day

177   starting from June 1, first with no aerosol (NA) effects, which is still the common practice for

178   most numerical weather forecasts in monsoon regions (Krishnamurti et al. 1991). A second

179   identical set of experiments was carried out but with the inclusion of aerosol radiative (RAD)

180   effect.   A third set of experiments same as the control, except with both aerosol radiative and

181   microphysics interactive effects (RADM) were carried out for the onset period June 11- 17.

182   Initial and boundary conditions for meteorology and aerosols were obtained respectively

183   from NCEP GFS 1° x1° global analysis, and from GOCART. By comparing the RAD and

184   RADM to NA forecasts over the NIHF region in a realistic setting with a high-resolution

185   regional model and sophisticated aerosol physics, we can gain a better understanding of

186   intrinsic, aerosol-monsoon interaction for the Indian monsoon, involving no change in

187   anthropogenic aerosol emissions.   In following discussions, all model anomaly quantities are

188   defined with respect to NA.   For brevity, we shall refer to RAD anomalies as due to Aerosol-

189   Radiative Interaction (ARI) effects.   Effects of Aerosol-Cloud-microphysics-Interaction

190 (ACI) will be diagnosed from comparison between RADM and RAD anomalies.   Aerosol

191 impacts will be examined using two different kinds of averaging. First, ensemble forecast

192 averaging for day-1 through day-7 for a specific date, will be compared to observation to

193 assess aerosol impacts on forecast skills. Second, ensemble averages of all forecasts as a

194 function of forecast days, will be used to assess the aerosol impact as a function of forecast

195 lead time.   For comparing model results to observations, we use rainfall data from the

196 Tropical Precipitation Measuring Mission (TRMM), and winds and temperature data from

197 the NASA MERRA2, Modern Era Retrospective analysis for Research and Applications -

198 version 2 (Bosilovich et al. 2015).

199

200 **3. Results**

201   To facilitate comparison of model results to observations, and set the stage for the

202 model output analysis, a brief description of the observed large-scale features of the Indian

203 monsoon of 2008 is presented first.

204 *3.1 Observed large-scale monsoon features during June 2008*

205   The excessive rainfall over northern India in June 2008 (see Fig. 1) was accompanied

206 by an upper tropospheric (500-200 hPa) anomalous warming (deviation from climatological

207 mean) northwest of the Indian subcontinent, and an anomalous large-scale anticyclone (Fig.

208 2a), with strong easterlies over northern Indian and the Arabian Sea (20-35 N), consistent

209 with thermal wind balance in an environment with positive temperature gradient (warmer-

210 north and colder-south).   The importance of the tropospheric temperature gradient in

211 controlling the timing of the onset of the Indian monsoon is well known (Li and Yanai 1996;

212 Goswami and Xavier 2005; Wu et al. 2012). In the lower troposphere, an anomalous low-

213   level cyclonic circulation cell was found over the northern Arabian Sea, coupled with an

214   anticyclonic cell over southeastern India and the southern Bay of Bengal (Fig. 2b).

215   Associated with these circulation cells were stronger low-level northeasterlies over the

216   Arabian Peninsular and strengthened low-level southwesterlies over the Arabian Sea and

217   westerlies over central India.   The former would increase dust emission over the desert

218   surface, and the latter would increase dust and moisture transport from the Arabian Sea to

219   northern India. Strong anomalous cooling of the lower troposphere was found over the Indo-

220   Gangetic Plain (20-30°N), and anomalous warming above with maximum upper troposphere

221   warming anchored over the Tibetan Plateau (Fig. 2c).   These features were accompanied by

222   anomalous ascending motions and increased water vapor over the NIHF with sinking motion

223   and increased dryness over southern India, and northern Indian Ocean (Fig.2 c, d).

224   Increased monsoon westerlies were found in the lower troposphere over central and Northern

225   India, and enhanced easterlies, from the upper troposphere to near surface over the NIHF

226   (Fig. 2d).   The aforementioned anomalies signal an enhancement of the early part of the

227   Indian monsoon consistent with the EHP effect due to dust aerosols (Lau et al. 2006, 2008;

228   Lau and Kim 2006).   It should be noted that spring and summer of 2008 coincided with the

229   decay phase of the 2007-2008 La Nina, with significant anomalous cooling over the

230   equatorial central and eastern Pacific and warming of the southern tropical Indian Ocean

231   during the boreal spring and summer of 2008. These SST anomalies would have

232   significantly influenced the aforementioned anomalies of the Indian monsoon (Rao et al.

233   2010; Kim et al. 2015). However, given the prescribed observed SST in the control

234   experiment (NA), SST effects including possible impacts of aerosols on SST are already

235   included in the prescribed observed SST and lateral boundary conditions in NA. Hence

236   model differences (with respect to NA) will only be attributed to aerosol effects associated

237   with aerosol-monsoon interaction on fast times scales, up to 7 days - the longest lead time

238   chosen for the model forecast experiments.

239

240   *3.2 Impact on model forecasts*

241   Figure 3 compares the distribution of AOD, rainfall and 850 hPa winds in NA with

242   observed rainfall from TRMM, AOD from MODIS, and winds from MERRA2 for the onset

243   phase of the 2008 Indian monsoon (June 11-17). The NA experiment simulates the mean

244   spatial distribution of aerosol AOD reasonably well compared to MODIS, featuring relatively

245   high aerosol loading over the northern Arabian Sea, and northwestern Indo-Gangetic Plain,

246   and low aerosol loading over northeastern India and the Bay of Bengal (Fig. 3). Overall, the

247   AOD magnitude is underestimated, in some regions with only half the magnitude of MODIS

248   AOD. An examination of the aerosol composition in GOCART has determined that a large-

249   fraction of the AOD over the Arabian Sea and northwestern India and Pakistan is contributed

250   mainly by desert dust (65-70%) transported from the Middle East deserts and the Thar desert

251   of northwestern Indian subcontinent.

252   The model mean rainfall and wind patterns show broad similarities to observations

253   (Fig. 3c, d), but with notable differences. The model low-level westerlies are too strong. As

254   a result, precipitation upwind over the mountain ridges of the Western Ghats, and Indo-China

255   are overestimated. The model also missed the heavy rainfall band extending from the east

256   coast of northern India into the Bay of Bengal. These are mostly due to the excessive

257   monsoon low-level westerlies across central and southern India. As shown in following

258   discussion, these biases are not related to model aerosol physics, because they are essential

259   unchanged in the RAD and RADM simulations. Another notable feature is the excessive

260   model rainfall over the southern Indo-Gangetic Plain, and deficient rainfall over the HF

261   compared to TRMM. In the following, we will demonstrate how this bias is mitigated in the

262   RAD and RADM experiments and how we can use the incremental improvement to explore

263   the physical processes underlying aerosol-monsoon interactions over NIHF region.   Despite

264   the aforementioned discrepancies, the overall AOD and rainfall distributions in the model are

265   consistent with dust aerosol emissions from the arid region of Southwest Asia, the Thar

266   desert, and Middle East deserts and transport across the Arabia Sea, with strong wet removal

267   in rainy regions.

268   Comparing the rainfall spatial distribution of RAD, and difference between RAD and

269   NA (Fig. 4a, b) depicts a shift of the monsoon rain band from NI to HF during the onset

270   phase, but little differences elsewhere. This means that given the large-scale aerosol and

271   meteorological initial condition, aerosol-monsoon interaction effects are mostly found over

272   the NIHF region.   The latitudinal rainfall profile averaged over the 80-90$^{\rm o}$E sector shows

273   clearly that the excessive NA model rainfall over the NI (23-25$^{\rm o}$N), and deficient rainfall

274   over the HF (25-30$^{\rm o}$N) compared to TRMM (Fig. 4c and d). ARI effects (Fig. 4e) clearly

275   shift the onset maximum rainfall northward towards the HF, mitigating but not completely

276   removing the model rainfall bias.

277   To further assess the impacts of aerosol-monsoon interactions on the model forecasts,

278   Fig. 5 shows the time series of the 1-7 days forecast rainfall, for NA and RAD, and TRMM,

279   for the extended integration period through 1 June to July 15 over the northern domain (ND),

280   and the southern domain (SD), defined along the curvature of the Himalaya mountain range

281   (see domain marker in Fig. 4b) to better capture the rainfall anomaly along the HF, arising

282 from aerosol-monsoon interaction. For the ND (Fig. 5a) the model forecasts show

283 reasonable skills in capturing the major episodes of heavy rainfall events. However, after the

284 onset, the model rainfall events tend to be overly active, with only much shallower breaks

285 compared to TRMM observations. It is also noted that clear differences between RAD and

286 NA forecasts tend to emerge after forecast day 3-4, when the control by the initial conditions

287 on the model forecasts are beginning to diminish. Beyond forecast day-4, the number of days

288 with predicted increased rainfall is much higher than that with reduced rainfall, in RAD

289 compared to NA, with a frequency ratio of approximately 2-to-1 indicating a strong impact

290 of absorbing aerosols in enhancing rainfall.   The time series of the Day 5-7 mean forecasts

291 (Fig 5b) show clear enhanced rainfall in RAD relative to NA, during the on-set phase of

292 rainfall events, indicating an advance (~ 1-5 days) of the onset of monsoon rainfall over the

293 ND (Fig. 5c) due to ARI. The rainfall enhancement and advance of rain events in ND can be

294 seen to last through the entire month of June and to early July. Conversely over SD (Fig. 5c),

295 rainfall is reduced in RAD compared to NA. Beyond forecast day-4, the number of days

296 with reduced rainfall compared that with increased rainfall is approximately 9 to 1, as a result

297 of the northward shift of convection and rainfall away from the SD to the ND. Note that the

298 SD experiences reduction in rainfall mostly during the peak and more often during the

299 dissipation phase of the rainfall events (Fig. 5d).

300

301 *3.3 Large-scale interactions*

302   In this section, we explore aspects of aerosol-monsoon large-scale interaction, which

303 governs the northward shift of rainfall from the SD to the ND.   The variations of anomalous

304 RAD rainfall and AOD are coherent (Fig. 6a), generally with enhanced rainfall in the ND

305 region (north of 27° N) where AOD is low, and suppressed rainfall in the regions of high

306 AOD in the SD (south of 27° N). This is consistent with increased wash out of aerosols in

307 wet regions, and longer aerosol life times in more stable dry regions. Wind anomalies (Fig.

308 6b) show a rapid strengthening and northward displacement of westerlies and southerlies in

309 the SD accompanying the monsoon onset over the ND, starting around June 16. This is

310 followed by a major event during June17-21 with increase in AOD, strengthening

311 southwesteries in the SD coupled to enhanced rainfall in the ND. A similar event involving

312 coherent variations of rainfall, AOD and winds took place during July 3-6. Note that

313 anomalous low-level southerlies after the monsoon onset (~June 16) remain unchanged in

314 sign, extending across approximately 27° N, from the SD to the ND. This means that the

315 ambient moisture in the SD is being advected northward by the strengthened southerlies, thus

316 increasing (decreasing) atmospheric moisture in the ND (SD). The resulting changes in

317 convective stability in terms of the vertical profiles of moist static energy in the two regions

318 will be discuss in Section 3.4. The aforementioned features indicate strong aerosol-

319 monsoon interactions associated with advection of aerosols and increased precipitation

320 downwind of the strengthening monsoon southwesterlies, consistent with EHP. The

321 fluctuations in AOD, winds, and rainfall in the ND and SD are associated with development

322 of westward propagating monsoon depression along the Himalayan foothills (See Section

323 3.4, for more detailed discussion). The overall aerosol radiation effects on the large-scale

324 monsoon environment are examined next.

325 The RAD anomalies of upper tropospheric temperature and winds (Fig. 7a) shows

326 clearly a warmer upper troposphere over northern India and regions further north with

327 increased upper level easterlies are found near 18-25°N induced by ARI. The upper level

14

328   anomalies are coupled to a strengthened low-level monsoon southwesterlies and a

329   pronounced increase in moisture over northwest and northern India (Fig. 7b). Reduced

330   moisture associated with the dry air masses and desert dust transport is found over the central

331   Arabian Sea, and northeastern India. Except for the magnitude, the anomaly patterns are

332   quite similar to those shown in Fig. 2a and b. As stated previously, SST effects are already

333   included in the prescribed observed SST. The present experiments are focused only on the

334   fast responses of aerosol-monsoon dynamic interaction. The results here suggest that ARI

335   reinforces, and adds regional details to, the SST forcing.

336   Additional regional features induced by aerosol radiative effects are depicted in

337   meridional-height anomaly cross-sections (Fig. 8). Over the Arabia Sea (60-70E), the dust

338   aerosol layer is thick, extending from the surface to 600 hPa, with maximum concentration in

339   the 800-700 hPa layer (Fig. 8a).   Pronounced atmospheric warming is found within the dust

340   layer, and cooling near the top of the dust layer mainly due to longwave radiation effects

341   (Zhang and Christopher 2003; Zhu et al. 2007; Lau et al. 2009). Substantial anomalous

342   warming is found over the upper troposphere 300-200 hPA layer, in conjunction with the

343   enhancement of the South Asian High and associated easterly warm advection (Fig. 7a).

344   Surface cooling is found over land surface north of 25° N, reflecting solar attenuation effects

345   due to aerosols (Ramanathan et al. 2005). The differential warming/cooling in the vertical

346   increases stability in the lower troposphere, but enhances instability above, giving rise to

347   weak rising motion in the mid- troposphere (Fig. 8c). As a result, except near the center of

348   dust layer, the atmosphere over the Arabian Sea is generally moister (Fig. 8b).   Given that

349   the same sea surface temperature is prescribed in all experiments, the source of moisture is

350   likely due to enhanced surface evaporation from the strengthened surface westerlies over the

351 Arabian Sea, as well as from increased mixing of the moist marine cloud water with

352 environmental air. Wind anomalies show increased easterlies (westerlies) in the upper

353 (lower) troposphere indicating a strengthening of the large-scale monsoon flow. The

354 colocation of low-level westerlies coincides with regions of maximum aerosol loading and

355 dry air masses signals strong westward advection of dust aerosols. As a result of the

356 aforementioned stability changes induced by ARI, an anomalous meridional circulation with

357 northward onshore flow towards southern Pakistan, and largely mid-tropospheric weak rising

358 motion is found over the region. This anomalous rising motion is likely to enhance

359 convective mixing and further moistening of the atmosphere over the ocean. However, the

360 region remains dry in the absolute sense, with no precipitation (Fig. 8d). Over the western

361 Indian region (70-80°E), the aerosol-monsoon characteristics are similar to those over the

362 Arabian Sea except that the signals are stronger, including a clear northward shift of the

363 center of moderate precipitation, accompanying a strengthening of the local monsoonal

364 meridional circulation (Fig. S2).

365 The ARI effects on precipitation and circulation are strongest over the domain

366 covering eastern India and the western Bay of Bengal (80-90° E). As shown in Fig. 8e, the

367 ARI-induced upper tropospheric warming over the Tibetan Plateau and regions to the south

368 are very pronounced. This occurs in conjunction with a pronounced elevated thick aerosol

369 layer, pushing against the southern slopes of the Tibetan Plateau by the increasing monsoon

370 southerlies (See Fig.6b). Here the dust loading is lower compared to that over the Arabian

371 Sea and western India, due to removal by both dry and wet depositions during the long-

372 distance transport from the Middle East deserts to eastern India. However, still noticeable

373 are the cooling near the top of the dust layer, warming within and below the dust layer and

374   near the surface, characteristic of light-absorbing dust layers [Zhu et al. 2007; Lau et al.

375   2009].   A signal of the aerosol semi-direct effect reducing convective potential, in the form

376   of strong surface cooling due to aerosol solar attenuation and warming induced by aerosol

377   heating can be found over the HF (25-35° N, Fig. 8e). However, this effect is overpowered

378   by the increased low-level moisture advection into this region by the strengthened

379   southwesterlies, as evident in the increased moist static energy in the lower troposphere

380   (700hPa) relative to the regions above (See discussion in Section 3.4, Fig. 11).   Except

381   within the dust layer, specific humidity is substantially increased over the entire atmospheric

382   column.   The increase is most pronounced and coincides with a strong low-level westerly jet

383   near 25-30N, (Fig. 8f). Coupled to the wind, temperature, moisture and aerosol anomalies,

384   is an enhanced local meridional circulation, with strong rising motion in the HF, and sinking

385   motion to the south (Fig.8g), and the northward displacement of the maximum rainfall over

386   the HF (Fig. 8h).

387

388   *3.4 Mesoscale Interactions*

389   In this section, we present results on the mesoscale aspects of aerosol-monsoon

390   interactions including both ARI and ACI effects, based on comparisons of the RADM, RAD

391   and NA experiments. Here, we focus on the evolution of mesoscale development of

392   monsoon rainfall systems during the onset phase (June 11-17) of the 2008 Indian monsoon.

393   As shown in Fig. 9 (panels in left column), in the absence of aerosol effects (NA), the onset

394   of the Indian monsoon over northern India was associated with increased transport of

395   moisture to the NIHF regions by the increasing monsoon southwesterlies, resulting in the

396   spontaneous development of a monsoon depression (cyclonic circulation cell) over the

397 northern Bay of Bengal as shown in the NA Day-4 forecast. At Day-5, a secondary cyclone

398 was spurred over the northern-central IGP. Subsequently, both monsoon cyclones amplified

399 and propagated northwestward, over the IGP. Such evolution of monsoon depressions is

400 well known during the monsoon onset, and active phases of the monsoon over northern India

401 [Krishnamurti and Bhalme 1976; Saha et al. 1981]. In RAD (panels in middle column), the

402 effect of ARI noticeable starting around Day-5, in a weakening of the primary monsoon

403 depression compared to NA, and in the development of intense small-scale convection cells

404 further northwestward up the HF. The suppression of the primary monsoon depression, and

405 the development of vigorous convective cells along the HF continue, with the most

406 pronounced signal at Day-7. In RADM (panels in right column), the inclusion of ACI

407 further enhances the ARI effects (See discussions related to Fig. 10 and 11). The suppression

408 of the primary monsoon onset cyclone is already noticeable at Day-4, and the subsequent

409 transformation (Day-5 to Day-7) of the monsoon onset cyclones (in NA) is similar to ARI

410 effects, except with faster speed, increased intensity and with more numerous convective

411 cells. The metamorphosis of the monsoon depression in NA to invigorated line precipitation

412 cells along the HF, due to combined effects of ARI and ACI is most striking at forecast Day-

413 7.

414   The invigoration of deep convection by ARI and ACI in the HF region is further

415 examined via the vertical distributions of hydrometeors associated with the deepening

416 convection in the ND and SD. Without aerosol effects (NA), the distributions of liquid

417 water (cloud and rain), cloud ice, snow and graupel indicate stronger development of deep

418 convection in SD than in ND (Fig. 10a, b). Comparing RAD (Fig. 10c, d) with NA (Fig.

419 10a, b), ARI shifts the maximum cloud ice upwards from 250 hPa to 200 hPa, enhances the

420 concentration of snow and graupel in the 500-300 hPa layer, and increases liquid water

421 content in the lower troposphere in the ND. In the SD, the effects are reversed, with

422 substantial reduction in deep convection as evidenced in substantial loss of cloud ice, and

423 snow and graupel in the mid to upper troposphere, as well as suppressed cloud and rain water

424 in the lower troposphere.   Comparing RADM (Fig. 10e, f) and RAD (Fig. 10c, d) anomalies

425 indicates that deep convection is further enhanced by ACI in ND, as evident in the larger

426 magnitude and extent of the increase in cloud ice, and snow/graupel in the mid- and upper

427 troposphere. This appears to be at the expense of reduced rate of increase in cloud and rain

428 water in the lower troposphere compared to RAD.   In the SD, the stronger reduction

429 hydrometeors of all kinds suggest a further suppression of deep convection by ACI. For the

430 domain as a whole, the change in total rainfall due to inclusion of ACI is relatively small

431 (<5%). Most of the changes by ACI appear to be in the nature of the deep convection and

432 not in the total rain.   These results are consistent with modeling and observations indicating

433 enhanced glaciation, and formation of deeper clouds by aerosols in a moist environment

434 [Rosenfeld *et al*. 2008, Fan *et al.* 2013].

435   The changes in the nature of the deep convection induced by ARI and ACI can be

436 viewed in terms of changes in moist static energy (MSE) of the atmosphere over the ND and

437 SD during the onset phase (Fig. 11).   Judging from the stronger negative gradient (reduction

438 with height) in mean MSE in the lower troposphere (Fig. 11a, b), it can be inferred that in the

439 absence of aerosol influence (NA), the SD is more (compared to the ND) convectively

440 unstable, and convection is likely to be deeper, as reflected in the larger loading of

441 hydrometeors of all types (Fig. 10a, b). Under ARI forcing, the lower troposphere in ND

442 (Fig. 11c, d) is further destabilized with increase in negative gradient MSE between 800 hPa

443   and 600 hPa, while the mid- to upper troposphere between 600-300 hPa are stabilized, as

444   evidence in the positive gradients in MSE between these two levels. Above 300 hPa, the

445   MSE reflects again a convective de-stabilization of the atmosphere. Computations of

446   separate contributions to the MSE (Fig. S3) shows that the destabilization in the lower

447   troposphere is mainly due to increased moisture, while stabilization is mainly due to

448   temperature change, *i.e.*, aerosol semi-direct effect in heating the lower troposphere and

449   cooling of the surface. Changes in MSE in the mid-to upper troposphere is associated with

450   temperature change due to moist adiabatic ascent of heated air from below reaching

451   maximum altitude.   Essentially, in the ND, the low-level moisture effect overpowers the

452   aerosol semi-effect, invigorating more intense convection and rainfall. Clearly, ACI

453   enhances the MSE convective stability modulation due to ARI, favoring enhanced deep

454   convection in ND (Fig. 11e).   In contrast, for the SD under ARI (Fig. 11f), both the aerosol

455   semi-direct effect and the reduction in moisture by advection (see discussion related to Fig.

456   7) stabilizes the lower troposphere, leading to the dissipation of the monsoon depression and

457   suppressed precipitation.   This effect is further amplified by ACI (Fig. 11f).   As noted

458   previously, the northward advection of the un-precipitated moisture from suppressed rainfall

459   in SD by the strengthened southerlies can further increase in convective instability and

460   rainfall in ND. This is the essence of the EHP effect.   Overall, it can be argued that the MSE

461   changes provide the physical underpinnings of anomalous deep convection, rainfall and

462   moisture transport induced by ARI and ACI in the NIHF region.

463

464   **4. Conclusions**

465   Using the NU-WRF model, we have conducted numerical forecast experiments to

466   investigate the dynamics of aerosol-monsoon interaction over the complex topography of the

467   NIHF region, under realistic initial and boundary conditions.   Results show that aerosol-

468   monsoon interactions have strong impacts on regional monsoon rainfall and circulation

469   during the onset phase of 2008 Indian monsoon, consistent with the EHP hypothesis.   Key

470   findings include:

471   • The complex and steep topography of the Himalaya foothills facilitate the build up of

472   thick layers of dust aerosols transported by monsoon southwesterlies from the Arabian

473   Peninsular deserts across the Arabian Sea, and accumulated over northwestern and central

474   India during the pre- and early monsoon season of 2008.

475   • Via aerosol induced dynamical feedback, ARI warms the upper troposphere over the

476   Tibetan Plateau, increases the mid-to-upper tropospheric north-south temperature gradient,

477   and thus strengthens the early Indian monsoon by shifting maximum monsoon rainfall

478   from the Indo-Gangetic Plain to the Himalayan foothills regions, and advancing the timing

479   of monsoon onset over HF by 1-5 days

480   • Aerosols have both local and non-local effects, which interacts with each other.

481   Generally, regions of high aerosol loading are associated with drier air masses and

482   suppressed rainfall, and heavy rain regions with low aerosol loading due to wash-out.

483   The semi-direct (local) effect of dust aerosols leads to the stabilization and weakening of a

484   developing monsoon depression over northeastern India and northern Bay of Bengal

485   during the onset phase of the monsoon.

486   • Non-local effects are exerted mainly through moisture and circulation feedback. Heating

487   by thick dust layer over the Arabian Sea and northern India, enhances the large-scale

488   southwesterly low-level monsoon flow and transport of moisture from the Arabian Sea to

489   the Indian subcontinent. The enhanced southwesterly moisture transport increases low-

490   level MSE, leading to the development of intense convective cells over the Himalaya

491   Foothill regions.

492   • While ARI dominates the large-scale aerosol-monsoon interaction, ACI further enhances

493   the ARI effects, by suppressing development of monsoon depression over northeastern

494   India, while intensifying the ice-phase precipitation and deep cloud processes in the HF,

495   and thereby speeding up the transformation the monsoon depression into intense meso-

496   scale cells with heavy rain in the forms line convection along the rugged terrains of the

497   HF.

498   Our results are in general agreement with recent modeling studies using the WRF-

499   CHEM. Krishnamurti *et al.* (2015) showed that the development of monsoon depression is

500   suppressed by aerosol via increased cloud condensation nuclei (CNN), over northeastern

501   India and Bay of Bengal.   However, their results did not indicate development of mesoscale-

502   scale deep convection over the Himalayan foothills, most likely because aerosol number

503   concentration was prescribed in their experiments, which therefore did not include the full

504   interactions of aerosol radiation, microphysics, and removal processes, with monsoon

505   dynamics. Jin et al. (2015) using WRF-CHEM and satellite observations also found that the

506   influx of Middle East dust, mainly through radiative forcing, could redistribute and increase

507   Indian summer monsoon regional rainfall, consistent with our results. However the relative

508   low resolution model (~35 km) they used would be unable to resolve the aerosol-monsoon

509   dynamic interaction over the complex topography of Himalayas regions. Moreover, they

510   focused on the mean response of the entire Indian monsoon season (June- August), while we

511 emphasize the short-term (< 7days) interactions during the onset phase of the monsoon.

512 We also note that, even with the 9-km resolution used our experiments, the resolution is still

513 relative coarse, in terms of realistic representation of aerosol-cloud microphysics.   Cloud

514 resolving scales (< 2-3 km) is highly desirable for better representation the interaction of

515 aerosol with the complex topography of the Himalaya foothills. However, for such high

516 resolution simulation, only short-term integrations, with single or few ensemble simulations

517 are feasible, because of the prohibitive computational demands. Furthermore, as noted in the

518 discussion in Section 3.2, while NUWRF simulated the AOD spatial distribution reasonably

519 well, the magnitude of the aerosol loading was significantly underestimated, compared to

520 MODIS observation.   Assuming that a heavier aerosol loading will produce stronger impacts

521 on monsoon, it is plausible that the present results may have underestimated the actual

522 impacts of aerosols in reality .

523   As a caveat, we note that our results are based on a singular monsoon year of 2008.

524 More studies need to be carried out to ascertain the robustness of the results. Nonetheless,

525 the fundamental physical processes revealed by this study, together with many recent studies

526 of aerosol impacts on monsoon weather and climate, lend support to the paradigm that

527 aerosol from natural sources is an essential components of the Asian monsoon climate,

528 affecting variability of the monsoon on diverse spatio-temporal scales [Lau 2016].

529 Finally, an important message from our study, consistent with many contemporary studies on

530 aerosol-monsoon interactions (See Li *et al*. 2016 for a comprehensive review), is *that*

531 *aerosol-monsoon interaction is important not only for climate change but also for short-term*

532 *weather (3-7 days) forecasts, and very likely for medium to long-term forecasts (> 7 days) as*

533 *well as seasonal-to-interannual predictions of the Asian monsoon.*

534

539

540 **Reference**

541 Andreae, M. O., and D. Rosenfeld, (2008), Aerosol–cloud–precipitation interactions. Part

542   1. The nature and sources of cloud-active aerosols. *Earth-Science Reviews*, **89**,

543   13–41.

544 Barros, A. P., and D. P. Lattenmaier (1994), Dynamic modeling of orographically induced

545   precipitation, *Rev. Geophys.*, 32, 265– 284.

546 Barros, A. P., and Timothy J. Lang (2003), Monitoring the Monsoon in the Himalayas:

547   Observations in Central Nepal, June 2001. *Mon. Wea. Rev.*,**131**, 1408–1427.

548 Boos, W., and Z. Kuang (2010), Dominant control of the South Asian monsoon by

549   orographic insulation versus plateau heating, *Nature, 463*, 218-222

550   doi:10.1038/nature08707.

551 Bosilovich, M. and coauthors (2015), MERRA-2: Initial Evaluation of the Climate.,

552   *Technical Report Series on Global Modeling and Data Assimilation, Ed. R.*

553   *Koster,* NASA/TM-2015-104606/Vol.43.

554 Chin M., D. A. Chu, R. Levy, L. Remer, Y. Kaufman, B. Holben, T. Eck, P. Ginoux, and

555   Q. Gao (2004), Aerosol distribution in the Northern Hemisphere during ACE-

556   Asia: Results from global model, satellite observations, and Sun photometer

557   measurements, *J. Geophys. Res.*, 109, D23S90,   doi:10.1029/2004GL02014.

558 Chin, M., T. Diehl, O. Dubovik, T. F. Eck, B. N. Holben, A. Sinyuk, and D. G. Streets

559   (2009), Light absorption by pollution, dust and biomass burning aerosols: A

560   global model study and evaluation with AERONET data, *Ann. Geophys.*, 27,

561   3439-3464.

562

563   Chin, M., T. Diehl, Q. Tan, J. M. Prospero, R. A. Kahn, L. A. Remer, H. Yu, A. M.

564   Sayer, H. Bian, I. V. Geogdzhayev, B. N. Holben, S. G. Howell, B. J. Huebert, N.

565   C. Hsu, D. Kim, T. L. Kucsera, R. C. Levy, M. I. Mishchenko, X. Pan, P. K.

566   Quinn, G. L. Schuster, D. G. Streets, S. A. Strode, O. Torres, and X.-P. Zhao

567   (2014), Multi-decadal variations of atmospheric aerosols from 1980 to 2009 : a

568   perspective from observations and a global model, *Atmos. Chem. Phys.*, 14, 3657-

569   3690.

570   Collier and G. J., Zhang (2009)Aerosol direct forcing of the summer Indian monsoon as

571   simulated by the NCAR CAM3. *Clim Dyn* 32: 313. doi:10.1007/s00382-008-

572   0464-9

573   D'Errico, M., C. Cagnazzo, P. G. Gogli, et al., 2015: Indian monsoon and the elevated-

574   heat pump mechanism in a coupled aerosol-climate model. *J. Geophys. Res.*, 120,

575   8712–8723, doi:10.1002/2015JD023346.

576   Das, S., U. C. Mohanty, A. Tyagi, D. R. Sikka, P. V. Joseph, L. S. Rathore, A. Habib, S.

577   K. Baidya, K. Snam and A. Sarkar (2014), The SAARC STORM: A

578   coordinated filed experiment on severe Thunderstorm obsevations and regional

579   modeling over the South Asian region. *Bull. Am. Meteor. Soc.*, 603-617,

580   DOI:10.1175/BAMS-D-12-00237.1

581   Demott, P. J., A. J. Prenni, X. Liu, S. M. Kreidenweis, M. D. Petters, C. H. Twohy, M. S.

582   Richardson, T. Eidhammer , and D. C. Rogers (2010), Predicting global

583   atmospheric ice nuclei distributions and their impacts on climate. *Proc. Natl.*

584   *Acad. Sci.*, **107 (25)**, 11217–11222.

585   Eck, T. F., et al. (2010), Climatological aspects of the optical properties of fine/coarse

586   mode aerosol mixtures, *J. Geophys. Res.*, 115, D19205,

587   doi:<u>10.1029/2010JD014002</u>.

588   Fan, J., L. R. Leung, D. Rosenfeld, Q. Chen, Z. Li, J. Zhang, and H. Yan (2013),

589   Microphysical effects determine macrophysical response for aerosol impacts on deep

590   convective clouds, *Proc. Natl. Acad. Sci. U. S. A.*, *110*, E4581–90,

591   doi:10.1073/pnas.1316830110.Gadgil, S., et al. (2003), The Indian monsoon and its

592   variability precipitation fluctuations in the Nepal Himalaya and its vicinity and

593   relationship with some large-scale climatological parameters, *Annu. Rev. Earth*

594   *Planet. Sci*., 31, 429– 467

595   Ganguly, D., H. Gadhavi, A. Jayaraman, T. A. Rajesh, and A. Misra (2005), Single

596   scattering albedo of aerosols over the central India: Implications for the regional

597   aerosol radiative forcing, *Geophys. Res. Lett.*, *32*, doi:10.1029/2005GL023903.

598   Gillette, D. A., and R. Passi (1988), Modeling dust emission caused by wind eroson *J.*

599   *Geophys. Res.*, 93, 14233-14242.

600   Ginoux, P., M. Chin, I. Tegen, J. M. Prospero, B. Holben, O. Dubovik, and S.-J.

601   Lin (2001), Sources and distributions of dust aerosols simulated with the

602   GOCART model, *J. Geophys. Res.*, 106(D17), 20255–20273,

603   doi:<u>10.1029/2000JD000053</u>.

604   Goswami, B. N., and P. K. Xavier (2005), ENSO control on the south Asian monsoon

605   through the length of the rainy season, *Geophys. Res. Lett.*, 32, L18717,

606   doi:10.1029/2005GL023216.

607   Hazra, A., B. N. Goswami, and Jen-Ping Chen, 2013: Role of Interactions between Aerosol

608   Radiative Effect, Dynamics, and Cloud Microphysics on Transitions of Monsoon

609   Intraseasonal Oscillations. *J. Atmos. Sci.*, **70**, 2073–2087.

610   doi: http://dx.doi.org/10.1175/JAS-D-12-0179.1

611   Henriksson, S. V., J.-P. Pietikäinen , A.-P. Hyvärinen , P. Räisänen , K. Kupiainen, J.

612   Tonttila, R. Hooda , H. Lihavainen, D. O'Donnell , L. Backman , Z. Klimont , and

613   A. Laaksonen (2014), Spatial distributions and seasonal cycles of aerosol climate

614   effects in India seen in a global climate–aerosol model, *Atmos. Chem. Phys.*, 14,

615   10177–10192, 2014 www.atmos-chem-phys.net/14/10177/2014/ doi:10.5194/acp-

616   14-10177-2014

617   Houze, R. A., Wilton, D. C. and Smull, B. F. (2007), Monsoon convection in the Himalayan

618   region as seen by the TRMM Precipitation Radar. *Quart. J. Roy. Meteor. Soc.*,

619   133: 1389–1411. doi: 10.1002/qj.106

620   Jin, Q., J. Wei1 , Z.-L. Yang, B. Pu , and J. Huang (2015), Consistent response of Indian

621   summer monsoon to Middle East dust in observations and simulations, Atmos.

622   Chem. Phys., 15, 9897–9915, doi:10.5194/acp-15-9897-2015

623   Kim, M.-K., W. K.-M. Lau, K.-M. Kim, et al., 2015: Amplification of ENSO effects on

624   Indian summer monsoon by absorbing aerosols. *Climate Dyn.*, 1–15, doi:

625   10.1007/s00382-015-2722-y.

626   Koehler, K. A., S. M. Kreidenweis, P. J. DeMott, A. J. Prenni, C. M. Carrico, B. Ervens,

627   and G. Feingold (2006), Water activity and activation diameters from

628   hygroscopicity data — Part II: Application to organic species. *Atmos. Chem.*

629   *Phys.*, **6**, 795–809.

630

631   Krishnamurti, T. N., Xue, J., Bedi, H. S., Ingles, K. and Oosterhof, D. (1991), Physical

632   initialization for numerical weather prediction over the tropics. *Tellus* B, 43: 53–

633   81. doi: 10.1034/j.1600-0889.1991.t01-2-00007.x

634   Krishnamurti, T. N., and H. Bhalme (1976), Oscillations of a monsoon system. Part I:

635   Observational aspects. *J. Atmos. Sci*., 33, 1937–1954.

636   Krishnamurti T.N., A. Martin, R. Krishnamurti, A.Simon, A. Thomas, V. Kumar (2013),

637   Impacts of enhanced CCN on the organization of convection and recent reduced

638   counts of monsoon depressions. *Clim. Dyn*. 41:117-134, doi 10.1007/s00382-

639   012-1638-z.

640   Lang, S., W.-K. Tao, J.-D. Chern, D. Wu, and X. Li (2014), Benefits of a 4th ice class in

641   the simulated radar reflectivities of convective systems using a bulk microphysics

642   scheme, *J. Atmos. Sci.,***71**, 3583-3612.

643   Lau, W. K. M. (2016), The Aerosol-Monsoon Climate System of Asia: A New Paradigm.

644   *J. Meteor. Res.*, 29(6), doi: 10.1007/s13351-015-5999-1.

645   Lau, W. K. M. (2014), Desert Dust and Monsoon Rainfall, *Nature, Geoscience*

646   doi:10.1038/ngeo2115

647   Lau, K. M., and K. M. Kim (2006), Observational relationships between aerosol and

648   Asian monsoon rainfall, and circulation, *Geophys. Res. Lett.*. 33, L21810,

649   doi:10.1029/2006GL027546.

650   Lau, K. M., Kim, K. M., Sud, Y. C., and Walker, G. K. (2009), A GCM study of the

651   response of the atmospheric water cycle of West Africa and the Atlantic to

652   Saharan dust radiative forcing, *Ann. Geophys.*, 27, 4023-4037, doi:10.51941

653   Angeo-27-4023-2009.

654   Lau, K. M., M. K. Kim, and K. M. Kim (2006), Aerosol induced anomalies in the Asian

655   summer monsoon: The role of the Tibetan Plateau. *Climate Dynamics*, **26** (7-8),

656   855-864, doi:10.1007/s00382-006-0114-z.

657   Lau, K.M, V. Ramanathan, G-X. Wu, Z. Li, S. C. Tsay, C. Hsu, R.Sikka, B. Holben, D.

658   Lu, G. Tartari, M. Chin, P .Koudelova, H. Chen, Y. Ma, J. Huang, K. Taniguchi,

659   and R. Zhang.(2008) the Joint Aerosol-Monsoon Experiment: A New Challenge

660   in Monsoon Climate Research. *Bull. Am. Meteor. Soc*., **89**, 369-383,

661   DOI:10.1175/BAMS-89-3-369.

662   Li, C., and M. Yanai (1996), The onset and interannual variability of the Asian summer

663   monsoon in relationship to land-sea thermal contrast. *J. Climate,* 9, 358-374.

664   Li, Z., W.K.-M. Lau, V. Ramanathan, G. Wu Y. Ding, M.G. Manoj, J. Liu, Y. Qian, J. Li,

665   T. Zhou, J. Fan, D. Rosenfeld, Y. Ming, Y. Wang, J. Huang B. Wang, X. Xu, S.-

666   S., Lee, M. Cribb, F. Zhang, X. Yang, T. Takemura, K. Wang, X. Xia, Y. Yin, H.

667   Zhang, J. Guo, P.M. Zhai, N. Sugimoto, S. S. Babu, G.P. Brasseur. (2016),

668   Aerosol and Monsoon Climate Interactions over Asia. *Geophys. Rev*. (in press).

669   Liu, Y., and P. H. Daum (2004), Parameterization of the autoconversion process. Part I:

670   Analytical formulation of the Kessler-type parameterizations. *J. Atmos. Sci*, **61**,

671   1539-1548.Manoj, M. G., P. C. S. Devara, P. D. Safai (2011), Absorbing aerosols

672   facilitate transition of Indian monsoon breaks to active spells. *Climate Dyn*.,

673   37,2181–2198, doi:10.1007/s00382-010-0971-3.

674   Meehl, G., J. Arblaster, and W. Collins (2008), Effects of black carbon aerosols on the

675   Indian monsoon, *J. Climate*, *21*, doi:10.1175/2007JCLI1777.1.

676   Peters-Lidard, C.D., E. M. Kemp, T. Matsui, J. A. Santanello, Jr., S. V., Kumar, J. P.

677   Jacob, T. Clune, W.-K. Tao, M. Chin, A. Hou, J. L. Case,, D. Kim, K.-M. Kim,

678   W. Lau, Y. Liu, J.-J. Shi, D. Starr, Q. Tan,, Z. Tao, B. F. Zaitchik, B. Zavodsky,

679   S. Q. Zhang, M. Zupanski (2015), Integrated modeling of aerosol, cloud,

680   precipitation and land processes at satellite-resolved scales, *Environmental*

681   *Modelling & Software*, **67**, 145-159

682   doi:http://dx.doi.org/10.1016/j.envsoft.2015.01.007

683   Peters-Lidard, P. R. Houser, Y. Tian, S. V., Kumar, J. Geiger, S. Olden, L. Lighty, B.

684   Doty, P. Dirmeyer, J. Adams, K. Michell, E. F. Wood, J. Sheffield (2007), High-

685   performance earth system modeling with NASA/GSFC's Land Information

686   System (LIS), *Innovations in Systems and Software Engineering*, 3, 157-165,

687   DOI:10.1007/s11334-007-0028-x.

688   Ramanathan, V., C. Chung, D. Kim, T. Bettge, L. Buja, J. T. Kiehl, W. M. Washington,

689   Q. Fu, D. R. Sikka, and M. Wild (2005), Atmospheric brown clouds: Impacts on

690   South Asian climate and hydrological cycle, *Proc. Natl. Acad. Sci. USA*, *102*, 5326-

691   5333, doi:10.1073/ pnas.0500656102.

692   Randles, C. A., and V. Ramaswamy (2008), Absorbing aerosols over Asia: A

693   Geophysical Fluid Dynamics Laboratory general circulation model sensitivity study

694   of model response to aerosol optical depth and aerosol absorption, *J. Geophys. Res.*,

695   *113*, doi:10.1029/2008JD010140.

696   Rao, S. A., H. S. Chaudhari, S. Pokhrel, and B. N. Goswami (2011), Unusual central Indian

697   drought of summer monsoon 2008: Role of Southern Tropical Ocean Warming, *J.*

698   *Climate,* 23, 5163-5174, DOI:10.1175/2010JCL3257.1

699   Rasmussen, K. L., and R.A. Houze Jr. (2012), A Flash-Flooding Storm at the Steep Edge of

700   High Terrain: Disaster in the Himalayas. *Bull. Amer. Meteor. Soc.*, **93**, 1713–1724.

701   Rosenfeld, D., U. Lohmann, G. B. Raga, C. D. O'Dowd, M. Kulmala, S. Fuzzi, A. Reissell,

702   and M. O. Andreae (2008), Flood or drought: how do aerosols affect precipitation?,

703   *Science*, *321*, doi:10.1126/science.1160606.Saha, K., F. Sanders, J. Shukla (1981),

704   Westward propagating predecessors of monsoon depressions. *Mon. Wea. Rev.,* 109,

705   330-343.

706   Sanap, S. D., and G. Pandithurai. (2015), The effect of absorbing aerosols on Indian

707   monsoon circulation and rainfall: A review. *Atmospheric Research*.

708   Satheesh, S. K., K. Krishna Moorthy, S. Suresh Babu, V. Vinoj, and C. B. S. Dutt (2008),

709   Climate implications of large warming by elevated aerosol over India, *Geophys. Res.*

710   *Lett.*, *35*, doi:10.1029/2008GL034944.

711   Shi, J. J., T. Matsui, W.-K. Tao, C. Peters-Lidard, M. Chin, Q. Tan, K. Pickering, N.

712   Guy, S. Lang, and E. Kemp (2014), Implementation of an Aerosol-Cloud

713   Microphysics-Radiation Coupling into the NASA Unified WRF: Simulation

714   Results for the 6-7 August 2006 AMMA Special Observing Period. *Quart. J. Roy.*

715   *Meteor. Soc.*, **140**, 2158-2175, doi:10.1002/qj.2286

716   Tao, W.-K., D. Anderson, J. Chern, J. Estin, A. Hou, P. Houser, R. Kakar, S. Lang, W.

717   Lau, C. Peters-Lidard, X. Li, T. Matsui, B.-W. Shen, J.-J. Shi, and X. Zeng, 2009:

718   Goddard Multi-Scale Modeling Systems with Unified Physics, *Annales*

719   *Geophysics*, **27**, 3055-3064.

720   Tao, W.-K., J.-P. Chen, Z. Li, C. Wang, and C. Zhang (2012), Impact of aerosols on

721   convective clouds and precipitation, *Rev. Geophys*., 50, RG2001,

722   doi:10.1029/2011RG000369.

723   Tao, Z., J. A. Santanello, M. Chin, S. Zhou, Q. Tan, E. M. Kemp, and C. D. Peters-Lidard

724   (2013), Effect of land cover on atmospheric processes and air quality over the

725   continental United States – a NASA Unified WRF (NU-WRF) model study, Atmos.

726   Chem. Phys., 13, 6207–6226.Tyagi, A., H. R. Hatwar and D. S. Pai, 2009: Monsoon

727   2008: A Report. National Climate Centre, *Indian Met. Dept., Monograph,*

728   *Synoptic Meterorology* No: 07/2009

729   Vinoj, V., P. J. Rasch, H. L. Wang, et al. (2014), Short term modulation of Indian

730   summer monsoon rainfall by West Asian dust. *Nat. Geosci*., **7**, 308–313,

731   doi:10.1038/NGEO2107

732   Wang, C., D. Kim, A. M. L. Ekman, M. C. Barth, and P. J. Rasch (2009), Impact of

733   anthropogenic aerosols on Indian summer monsoon, *Geophys. Res. Lett*., 36,

734   L21704, doi:10.1029/2009GL040114.

735   Wu, G., Y Liu, B. He, Q. B, A. Duan, F. F. Jin, (2012),   Thermal controls on the Asian

736   Summer Monsoon,   *Sci. Reports*, 404, doi:10.1038/srep00404

737   Zhang, J., and S. A. Christopher (2003), Longwave radiative forcing of Saharan dust

738   aerosols estimated from MODIS, MISR, and CERES observations on

739   Terra*, Geophys. Res. Lett.,* 30, 2188, doi:10.1029/2003GL018479, 23.

740   Zhu, A., V. Ramanathan, F. Li, and D. Kim (2007), Dust plumes over the Pacific, Indian,

741   and Atlantic oceans: Climatology and radiative impact, *J. Geophys. Res*., 112,

742   D16208, doi:10.1029/2007JD008427.

743

744   **Figure Caption**

745   Figure 1   Spatial distribution of   observed a) rainfall anomalis (mm day^{-1}) from TRMM

746   and b) AOD from MODIS, for the Indian monsoon during June 2008.   Rainfall

747   anomalies are computed related to 1998-2013 climatology.

748   Figure 2   Horizontal distribution of anomalies of a) tropospheric temperature (^{o}C) and

749   winds (ms^{-1}) averaged between 500-200 hPa , b)850 hPa winds and specific

750   humidity (gKg^{-1}) in the lower troposphere (1000-600hPa; and latitude-height

751   cross-sections of c) meridional overturning circulation (streamline) and

752   temperature, and d) zonal winds (contour) and specific humidity.

753   Figure 3   Horizontal distribution of AOD a) in control model simulation (NA), and b)

754   from MODIS observation.   Rainfall and winds in c) NA experiment, and b) from

755   TRMM, and MERRA2.   Unit of rainfall in mm day^{-1}, and winds in ms^{-1}.

756   Figure 4   Distribution of   a) total rainfall in RAD, b) rainfall anomalies in RAD.

757   Latitudinal profile of rainfall averaged between 80-90 E in c) TRMM

758   observations, d) NA, and e) RAD, with positive (negative) RAD-minus-NA

759   differences indicated by red (blue) shading. The boundaries of Northern and

760   Southern Domain defined based on local tropograhy used for later analysis are

761   also shown.

762   Figure 5 Time series of a) individual 7-day rainfall forecasts June 10-July 21 and b)

763   ensemble mean of Day5-Day7 forecasts for the Northern Domain, and same for

764   c) and d) except for the Southern Domain (See domain definition in Fig 4b).

765   Histogram in a) and c) indicates observed TRMM rainfall in the Northern Domain

766   and the Southern domain respectively. Red (blue) dots and shading indicate

767   enhanced (reduced) rainfall in RAD relative to NA.   Unit of rainfall in mmday^{-1}.

768   Figure 6 Latitude-time cross-section of ensemble mean forecasts during June 1- 17, 2008

769   for a) AOD (contour) and rainfall anomalies (in % change), and b) zonal wind

770   (shaded) and meridional wind (contour). Unit of wind in ms^{-1}.

771   Figure 7 Horizontal distribution of RAD anomalies in a) temperature averaged between

772   500-200 hPa and 200 hPa winds, and b) lower tropospheric moisture and winds

773   during June 10-17, 2008.

774   Figure 8 Height-latitude cross sections of a) temperature (color shaded) and AOT

775   (contoured), b) specific humidity (color shaded) and zonal wind (contoured), c)

776   meridional streamlines with vertical upward (downward) motions shaded red

777   (blue), and d) precipitation anomalies for the Arabian Sea-Pakistan-Afghanistan

778   region (60-70E).   Positive (negative) anomalies are indicated by solid (dashed)

779   contours, or red (blue) color.   Same for e), f), g) and h), except for the northern

780   and northeastern India sector.

781   Figure 9 Time sequence showing the genesis and evolution of monsoon rainfall and

782   mesoscale convective complex from forecast Day4 to Day 7, for a) NA, b) RAD

783   and c) RADM.   Extreme heavy precipitation (> 120 mm day^{-1}) is shaded red.

784   Figure 10   Time-height distribution of different hydrometeor species for a) the Northern

785   Domain in NA, and b) the Southern Domain in NA.   Same for c) and d), except

786   for the RAD anomalies, and same for e) and f), except for RADM anomalies.

787   Purple contour, color shading, and black contour denotes respectively

788   concentration of cloud-ice, snow and graupel, and liquid phase clouds and rain.

789   Positive (negative) anomalies in c) through f) are indicated either by solid

790   (dashed) contours or red (blue) shading.   Units are in 10^{-5} kg m $^{-3}$.

791   Figure 11 Vertical profile of MSE (KJ Kg^{-1}) showing a) mean distribution for the

792   Northern Domain and b) the Southern Domain. Same for c) and d) except for

793   RAD anomalies for forecast Day 6, and e) and f) except for RADM anomalies for
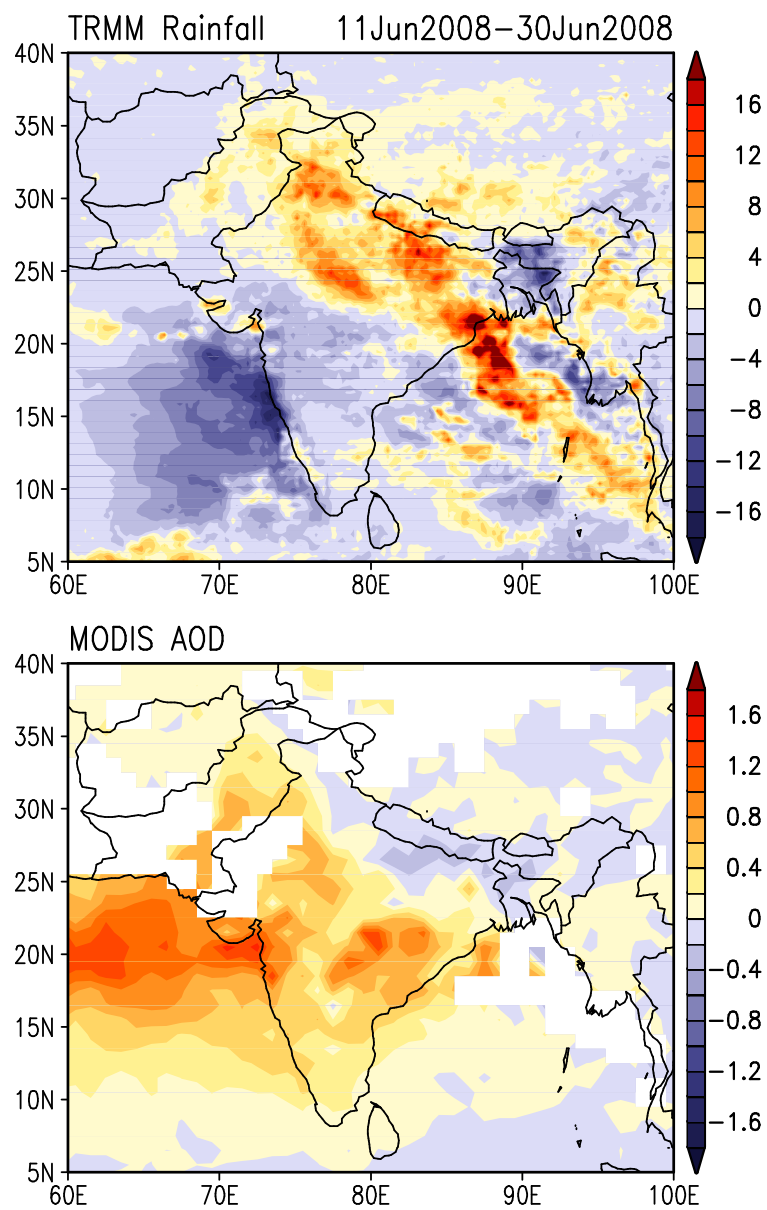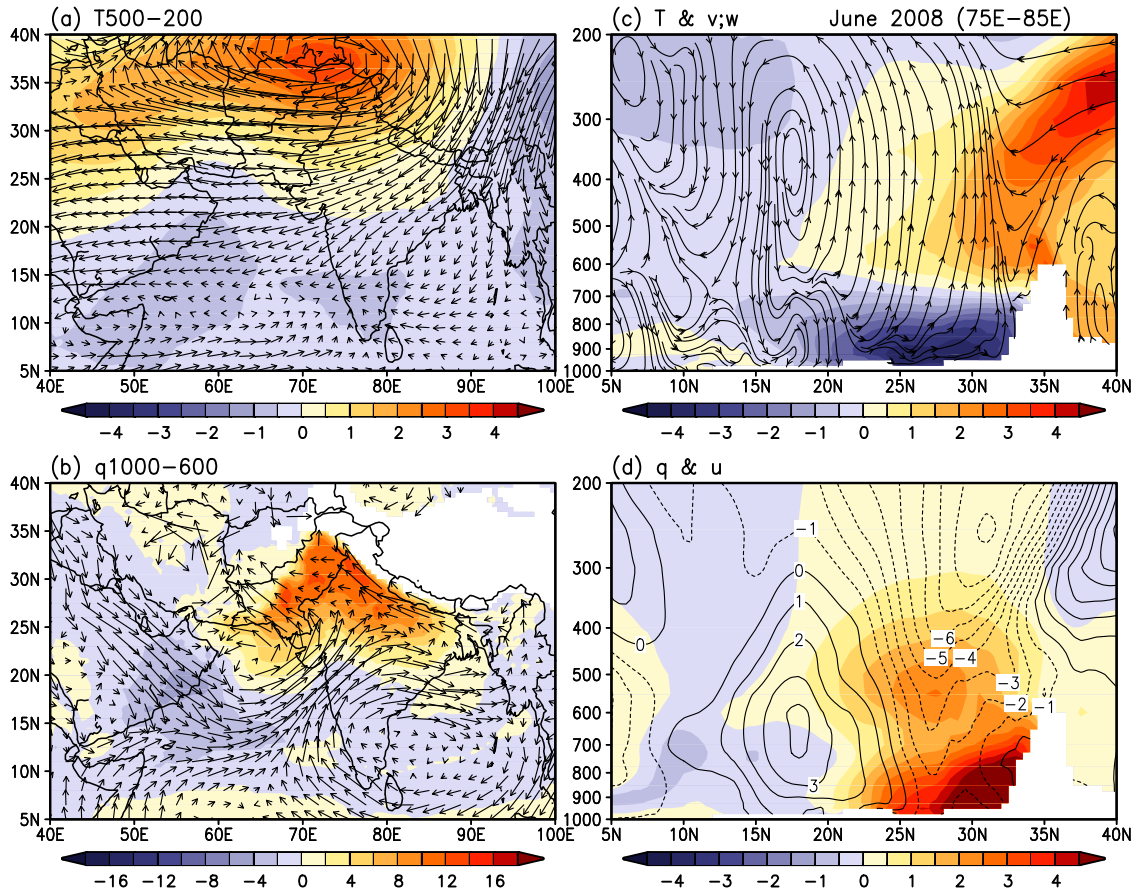
794   forecast Day 6.

795
796 Figure 1   Spatial distribution of   observed a) rainfall anomalis (mm day^{-1}) from TRMM
797   and b) AOD from MODIS, for the Indian monsoon during June 2008.   Rainfall
798   anomalies are computed related to 1998-2013 climatology.
799
800

801
802

(a) T500−200

(b) q1000−600

(c) T & v;w   June 2008 (75E−85E)

(d) q & u

803
804
805   Figure 2   Horizontal distribution of anomalies of a) tropospheric temperature (°C) and
806   winds (ms⁻¹) averaged between 500-200 hPa , b)850 hPa winds and specific
807   humidity (gKg⁻¹) in the lower troposphere (1000-600hPa; and latitude-height
808   cross-sections of c) meridional overturning circulation (streamline) and
809   temperature, and d) zonal winds (contour) and specific humidity.
810
811

812
813
814
815
816   Figure 3   Horizontal distribution of AOD a) in control model simulation (NA), and b)
817   from MODIS observation.   Rainfall and winds in c) NA experiment, and b) from
818   TRMM, and MERRA2.   Unit of rainfall in mm day^{-1}, and winds in ms^{-1}.
819
820
821
822
823
824
825
826
827

828
829
830

831
832
833
834   Figure 4   Distribution of a) total rainfall in RAD, b) rainfall anomalies in RAD.
835   Latitudinal profile of rainfall averaged between 80-90 E in c) TRMM
836   observations, d) NA, and e) RAD, with positive (negative) RAD-minus-NA
837   differences indicated by red (blue) shading. The boundaries of Northern and
838   Southern Domain defined based on local tropograhy used for later analysis are
839   also shown.

840
841
842
843
844
845
846
847
848
849
850
851

852
853

854
855

856 Figure 5 Time series of a) individual 7-day rainfall forecasts June 10-July 21 and b)
857   ensemble mean of Day5-Day7 forecasts for the Northern Domain, and same for
858   c) and d) except for the Southern Domain (See domain definition in Fig 4b).
859   Histogram in a) and c) indicates observed TRMM rainfall in the Northern Domain
860   and the Southern domain respectively. Red (blue) dots and shading indicate
861   enhanced (reduced) rainfall in RAD relative to NA.   Unit of rainfall in mmday^{-1}.
862

863
864
865
866

(a) % change in ensemble mean rainfall (shading) & AOD (contour)   (80E−90E)

(b) Zonal (shading) & Meridional (contour) winds at 850hPa

867
868
869
870   Figure 6 Latitude-time cross-section of ensemble mean forecasts during June 1- 17, 2008
871   for a) AOD (contour) and rainfall anomalies (in % change), and b) zonal wind
872   (shaded) and meridional wind (contour). Unit of wind in ms^{-1}.
873
874

875

876

Figure 7 Horizontal distribution of RAD anomalies in a) temperature averaged between
        500-200 hPa and 200 hPa winds, and b) lower tropospheric moisture and winds
        during June 10-17, 2008.

880

881
882

883
884
885 Figure 8 Height-latitude cross sections of a) temperature (color shaded) and AOT
886   (contoured), b) specific humidity (color shaded) and zonal wind (contoured), c)
887   meridional streamlines with vertical upward (downward) motions shaded red
888   (blue), and d) precipitation anomalies for the Arabian Sea-Pakistan-Afghanistan
889   region (60-70E).   Positive (negative) anomalies are indicated by solid (dashed)
890   contours, or red (blue) color.   Same for e), f), g) and h), except for the northern
891   and northeastern India sector.
892

893   Figure 9
894

895
896
897   Figure 9 Time sequence showing the genesis and evolution of monsoon rainfall and
898   mesoscale convective complex from forecast Day4 to Day 7, for a) NA, b) RAD
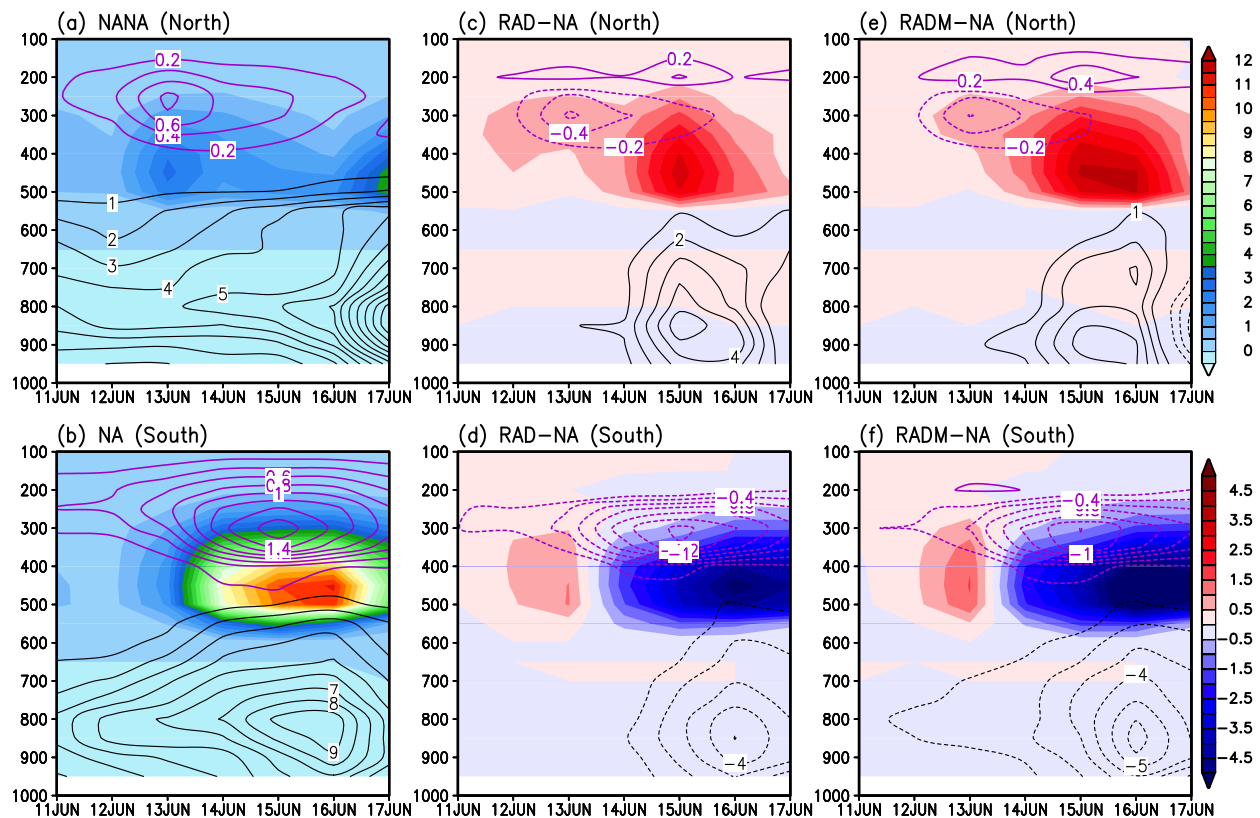899   and c) RADM.   Extreme heavy precipitation (> 120 mm day^{-1}) is shaded red.
900
901

Figure 10   Time-height distribution of different hydrometeor species for a) the Northern
Domain in NA, and b) the Southern Domain in NA.   Same for c) and d), except
for the RAD anomalies, and same for e) and f), except for RADM anomalies.
Purple contour, color shading, and black contour denotes respectively
concentration of cloud-ice, snow and graupel, and liquid phase clouds and rain.
Positive (negative) anomalies in c) through f) are indicated either by solid
(dashed) contours or red (blue) shading.   Units are in 10^{-5} kg m $^{-3}$.

914
915
916
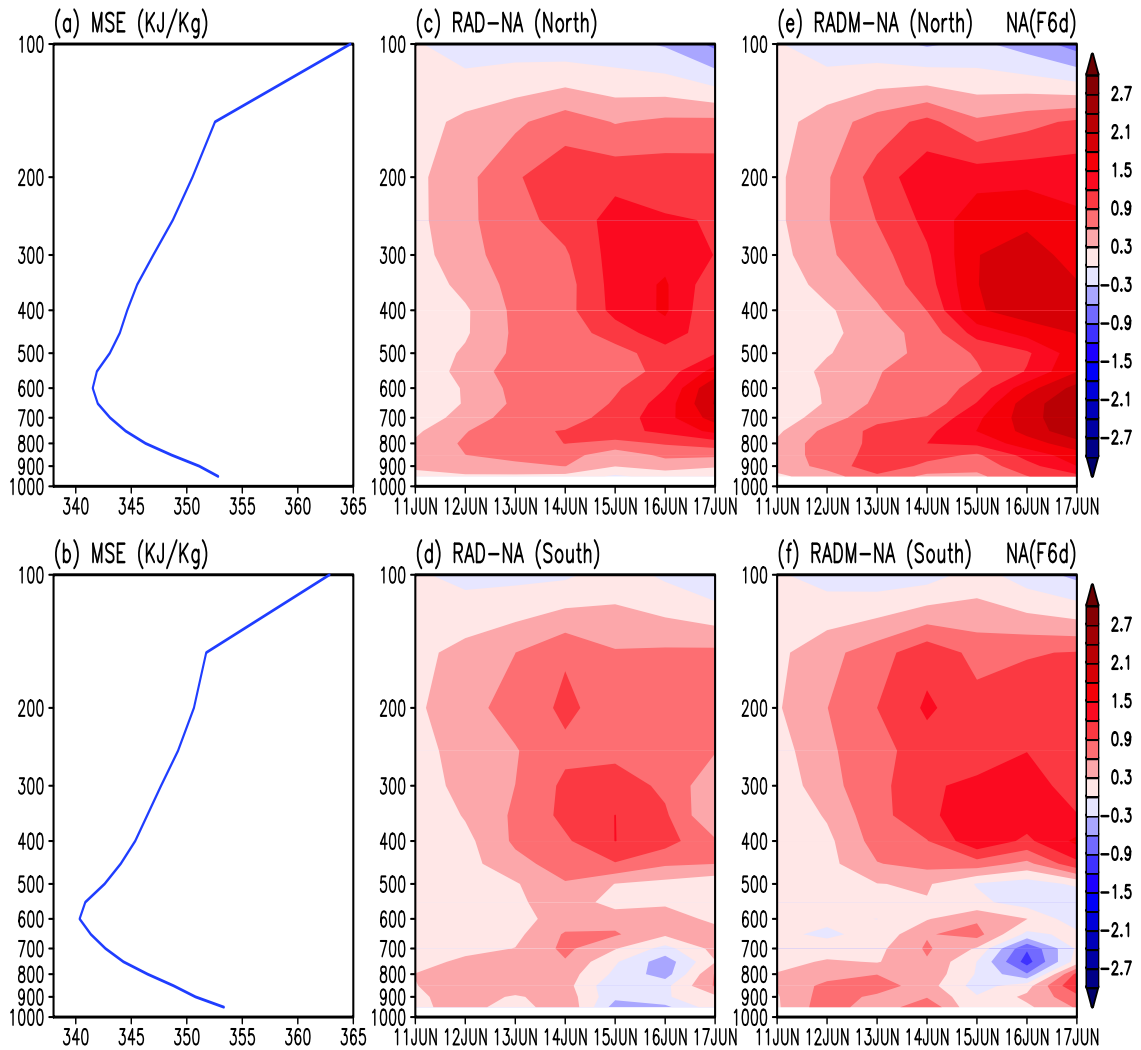
917
918
919   Figure 11 Vertical profile of MSE (KJ Kg^{-1}) showing a) mean distribution for the
920   Northern Domain and b) the Southern Domain. Same for c) and d) except for
921   RAD anomalies for forecast Day 6, and e) and f) except for RADM anomalies for
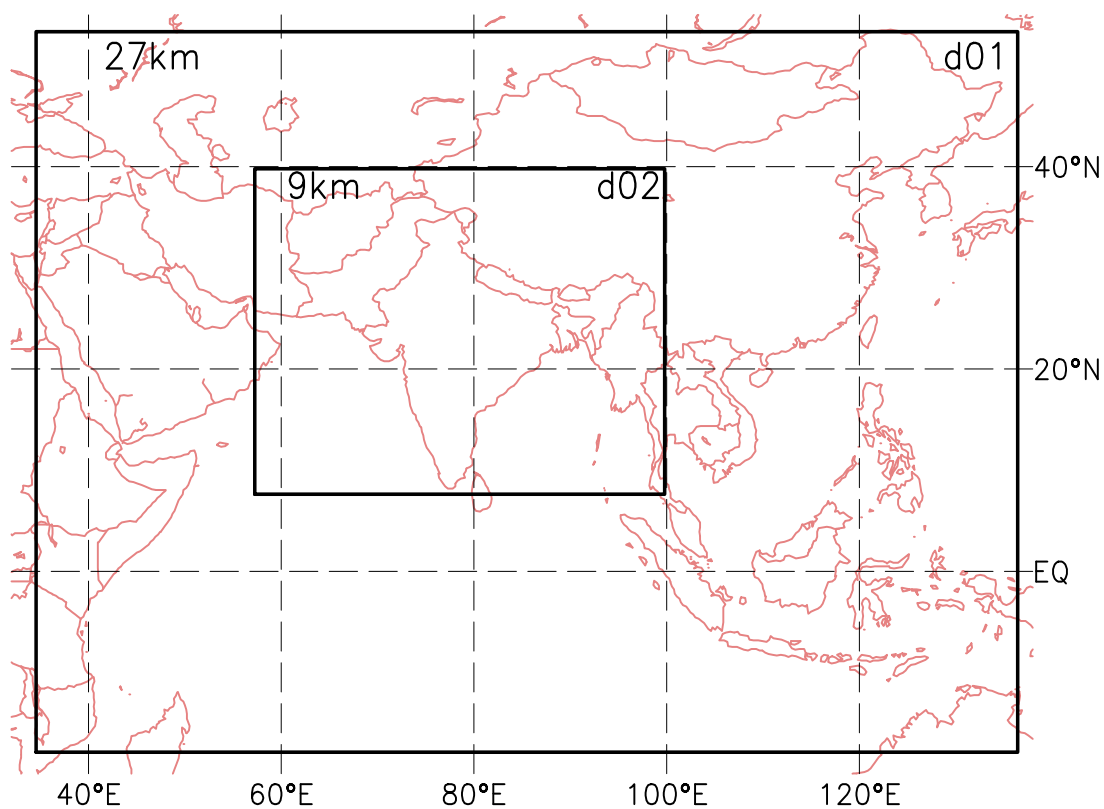922   forecast Day 6.
923

924   **Supplementary Material**
925

926

927   Figure S1 Nested domains used for NUWRF numerical experiments in this study.

928   The horizontal resolution is 9 x 9 km , and 27x27 km for the inner domain

929   and the outer domain respectively.

930   Figure S2   Height-latitude cross sections of a) temperature (color shaded) and AOT

931   (contoured), b) specific humidity (color shaded) and zonal wind (contoured), c)

932   meridional streamlines with upward (downward) motions shaded red (blue), and

933   d) precipitation anomalies for the Arabian Sea-Pakistan-Afghanistan region (70-

934   80° E).   Positive (negative) anomalies are indicated by solid (dashed) contours, or

935   red (blue) color.

936   Figure S3   Vertical profile of MSE anomalies for   a) the Northern Domain and b) the

937   Southern Domain at forecast Day-6.   Same for c) and d) except for contribution

938   by temperature, and for e) and f) except for contribution by moisture.

939

940

941

942

Figure S1 Nested domains used for NUWRF numerical experiments in this study.
The horizontal resolution is 9 x 9 km , and 27x27 km for the inner domain
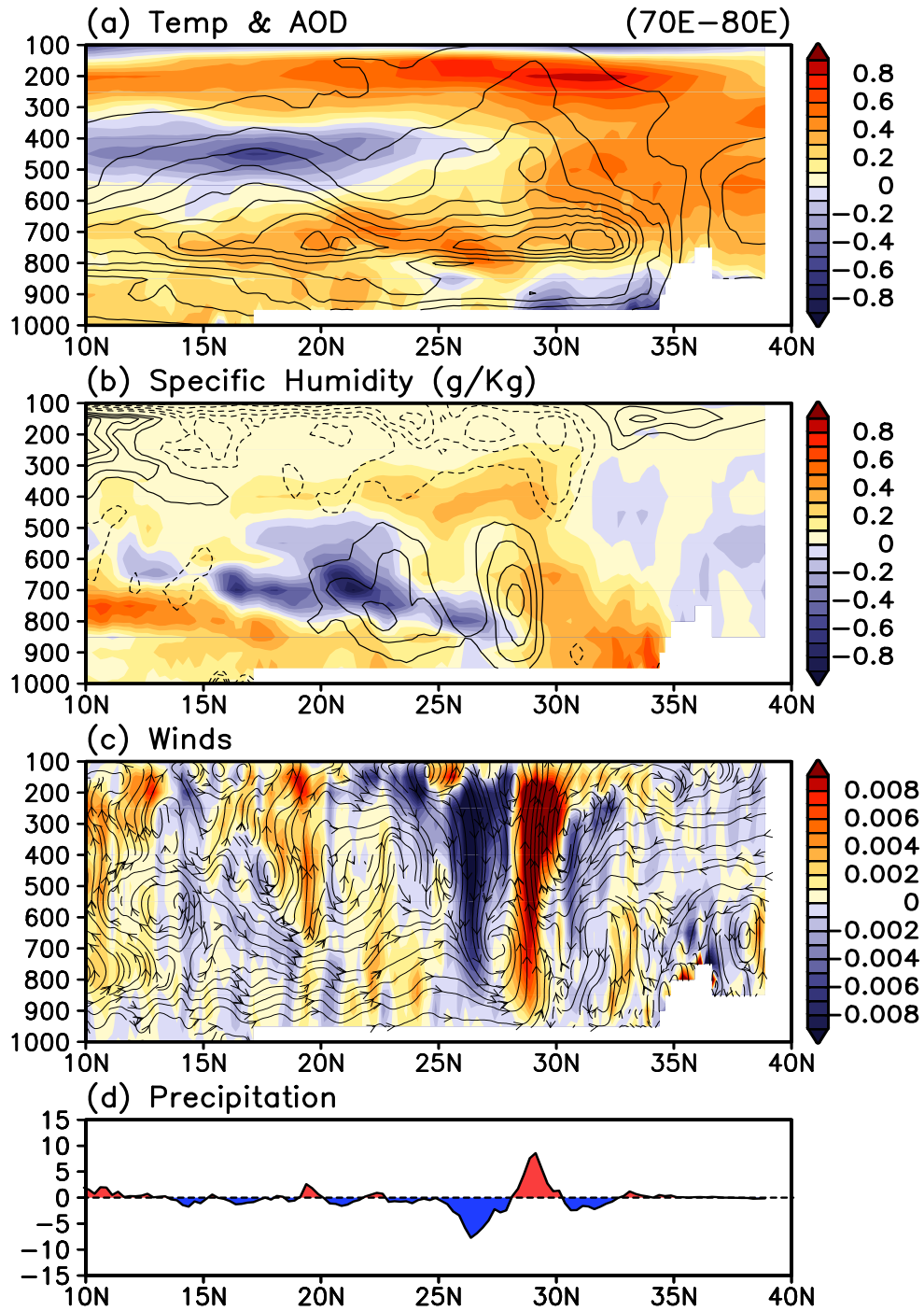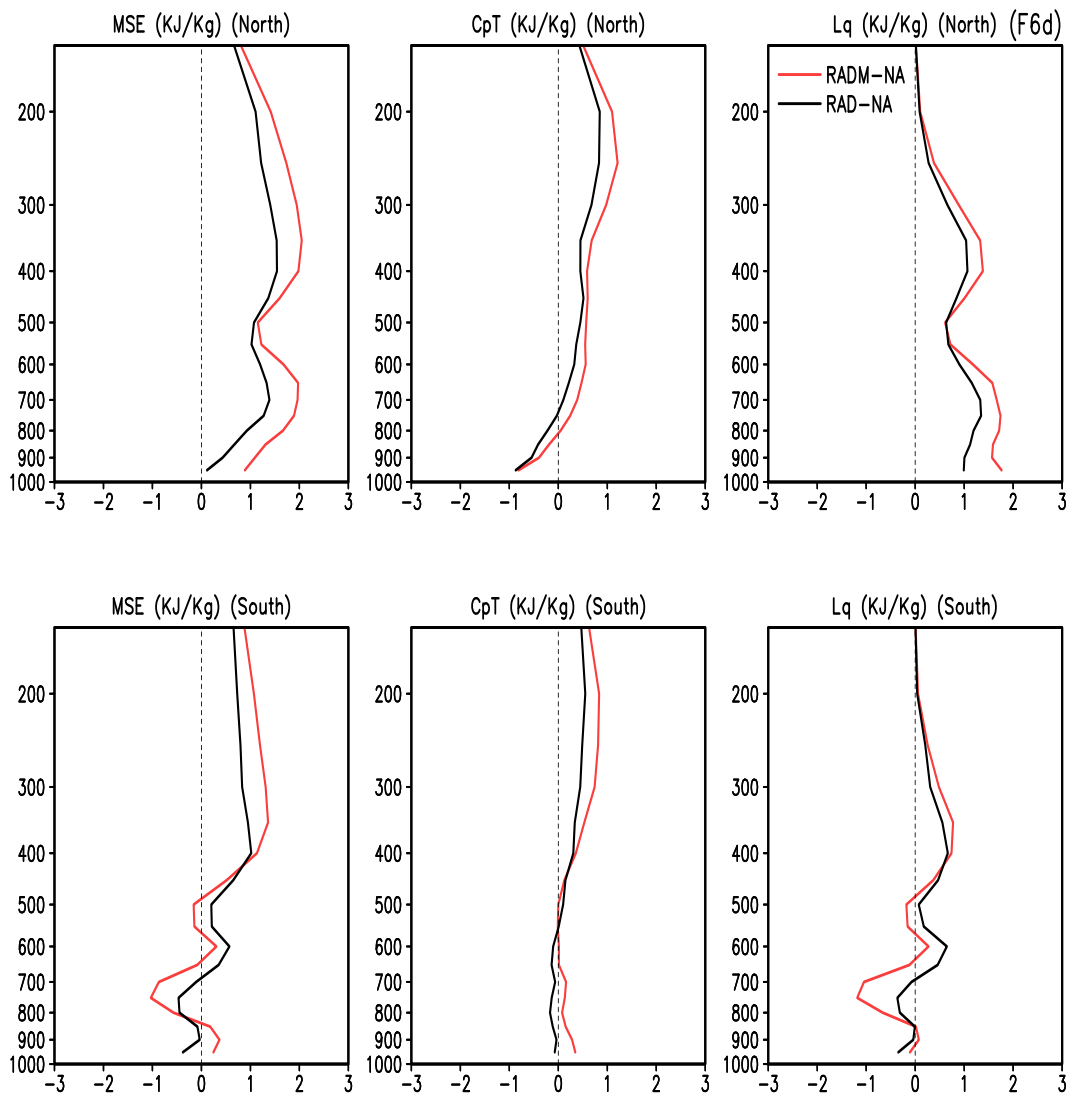and the outer domain respectively.

946

Figure S2 Height-latitude cross sections of a) temperature (color shaded) and AOT (contoured), b) specific humidity (color shaded) and zonal wind (contoured), c) meridional streamlines with upward (downward) motions shaded red (blue), and d) precipitation anomalies for the Arabian Sea-Pakistan-Afghanistan region (70-80° E). Positive (negative) anomalies are indicated by solid (dashed) contours, or red (blue) color.

954

955

Figure S3 Vertical profile of MSE anomalies for a) the Northern Domain and b) the
         Southern Domain at forecast Day-6.   Same for c) and d) except for contribution
         by temperature, and for e) and f) except for contribution by moisture.

959

960